

Strong Pauli-limiting behavior of H_{c2} and uniaxial pressure dependencies in KFe_2As_2

P. Burger,^{1,2} F. Hardy,¹ D. Aoki,^{3,4} A. E. Böhmer,^{1,2} R. Eder,¹ R. Heid,¹ T. Wolf,¹ P. Schweiss,¹ R. Fromknecht,¹ M. J. Jackson,⁵ C. Paulsen,⁵ and C. Meingast¹

¹*Institut für Festkörperphysik, Karlsruher Institut für Technologie, 76021 Karlsruhe, Germany*

²*Fakultät für Physik, Karlsruher Institut für Technologie, 76131 Karlsruhe, Germany*

³*INAC, SPSMS, CEA Grenoble, 38054 Grenoble, France*

⁴*IMR, Tohoku University, Oarai, Ibaraki 311-1313, Japan*

⁵*Institut Néel, CNRS and Université Joseph Fourier, BP 166, 38042 Grenoble Cedex 9, France*

(Dated: April 13, 2021)

KFe_2As_2 single crystals are studied using specific-heat, high-resolution thermal-expansion, magnetization, and magnetostriction measurements. The magnetization and magnetostriction data provide clear evidence for strong Pauli limiting effects of the upper critical field for magnetic fields parallel to the FeAs planes, suggesting that KFe_2As_2 may be a good candidate to search for the Fulde-Ferrell-Larkin-Ovchinnikov (FFLO) state. Using standard thermodynamic relations, the uniaxial pressure derivatives of the critical temperature (T_c), the normal-state Sommerfeld coefficient (γ_n), the normal-state susceptibility (χ), and the thermodynamic critical field (H_c) are calculated from our data. We find that the close relationship between doping and pressure as found in other Fe-based systems does not hold for KFe_2As_2 .

PACS numbers: 74.70.Xa, 74.25.Bt, 74.62.Fj

I. INTRODUCTION

The detailed understanding of Fe-based superconductors continues to present a considerable challenge in condensed matter physics.¹⁻⁴ Of particular interest recently has been the strongly hole doped compound KFe_2As_2 , which is the end member of the $(\text{Ba},\text{K})\text{Fe}_2\text{As}_2$ system and has a much lower T_c of only 3.4 K than the optimal T_c value of about 40 K near 40% K content.⁵⁻⁷ Whereas $\text{Ba}_{0.6}\text{K}_{0.4}\text{Fe}_2\text{As}_2$ appears to have a fully gapped s -wave order parameter,^{8,9} there are indications for a nodal superconducting state in KFe_2As_2 . In fact, a d -wave state was predicted early on from functional renormalization group theory.¹⁰ Experimentally, penetration depth and thermal conductivity studies have been interpreted in terms of a d -wave order parameter,^{11,12} whereas recent laser angle-resolved photoemission (ARPES) experiments suggest a nodal s -wave state.¹³ The electronic structure of KFe_2As_2 has been investigated both with de Haas-van Alphen (dHvA) and ARPES methods,^{6,14} and these studies show that KFe_2As_2 has only hole pockets. This of course immediately raises the question of whether superconductivity in KFe_2As_2 has the same mechanism as the optimally doped system, for which superconductivity has been suggested to originate from interband pairing between electron and hole pockets.⁴ Inelastic neutron scattering results still show signs of spin fluctuations, which are however incommensurate but may nevertheless lead to superconducting pairing in the heavily overdoped region.^{15,16} Paradoxically, KFe_2As_2 has the largest γ_n in the $(\text{Ba},\text{K})\text{Fe}_2\text{As}_2$ system in spite of the low T_c value, and this has been linked to a close proximity to an orbitally-selective Mott transition due to strong Hund correlations.^{17,18}

In this Article we study the normal- and superconducting-state properties of KFe_2As_2 using several thermodynamic probes: specific-heat, high-resolution thermal-expansion, magnetization, and magnetostriction measurements. Our magnetization and magnetostriction data clearly show that KFe_2As_2 is strongly Pauli limited for fields parallel to the FeAs planes and, thus, this system may be another possible candidate to search for the Fulde-Ferrell-Larkin-Ovchinnikov^{19,20} (FFLO) state. Using standard thermodynamic relations, the uniaxial pressure derivatives of the critical temperature (T_c), the normal-state Sommerfeld coefficient (γ_n), the normal-state magnetic susceptibility (χ), and the thermodynamic critical field (H_c) are calculated from our data. First, we find that the uniaxial pressure derivatives of T_c are very anisotropic and of opposite sign as compared to Co-doped Ba122 .²¹ We find that both T_c and γ_n decrease under hydrostatic pressure. This is in contrast to the doping induced behavior and shows that pressure and doping can not be equated, as they can in the Co- and P-doped Ba122 systems.^{22,23}

II. EXPERIMENTAL DETAILS

Single crystals of KFe_2As_2 were grown in alumina crucibles using a K-As rich flux with a K:Fe:As ratio of about 0.3:0.1:0.6. The crucibles were sealed in an iron cylinder filled with argon gas. After heating up to 980 °C the furnace was cooled down slowly at a rate of about 0.5 °C/h. Crystals with dimensions up to $3.0 \times 2.5 \times 1.0 \text{ mm}^3$ were used in the present investigation. The specific heat was measured with a commercial Quantum Design Physical Property Measurement System (PPMS) for $T > 0.4 \text{ K}$ and with a home-made calorimeter for

$T < 0.4$ K. For $T > 2$ K, we used a vibrating sample magnetometer to measure the magnetization. For $T < 2$ K, magnetization measurements were performed using a low-temperature superconducting quantum interference device (SQUID magnetometer) equipped with a miniature dilution refrigerator developed at the Institut Néel-CNRS Grenoble. The sample was attached to a copper press suspended from the dilution unit's mixing chamber which descends through the bore of the magnet. The magnetometer is equipped with a solenoid capable of producing fields up to 8 T. The setup can measure absolute values of the magnetization by the extraction method at temperatures down to 75 mK. The thermal expansion and the magnetostriction were measured in a custom-made capacitive dilatometer with a typical resolution of $\Delta L/L_0 \sim 10^{-8}$ - 10^{-10} .^{22,24}

III. RESULTS

A. Heat capacity

Figure 1 shows typical heat-capacity data of our samples, clearly demonstrating a sharp superconducting transition at $T_c = 3.4$ K and a large Sommerfeld coefficient $\gamma \approx 100$ mJ mol⁻¹ K⁻², as reported earlier.¹⁷ We attribute the decrease of C_p/T below about 0.5 K to small superconducting gaps on parts of the Fermi surface, which surprisingly appear to be absent in recent data.²⁵ In the following, we use the data of Fig. 1 for calculating the thermodynamical critical field (see Section III C) and the uniaxial pressure dependences (see Section IV B).

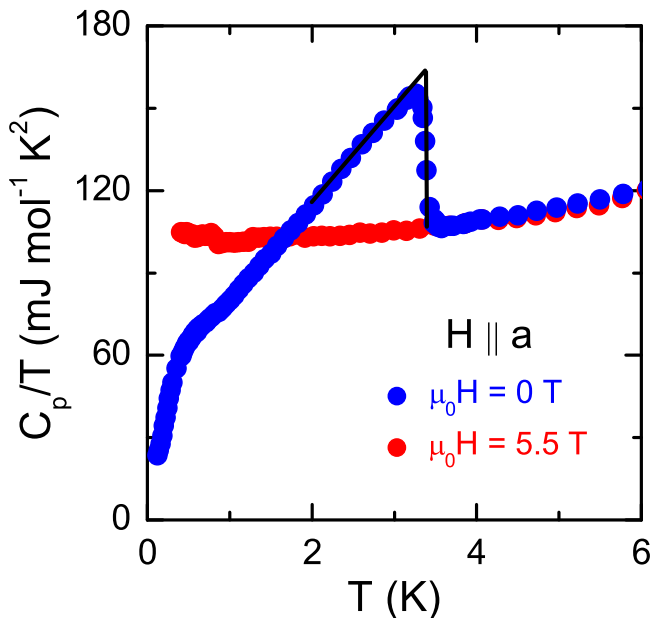


FIG. 1: (Color Online) Specific heat of KFe_2As_2 in 0 and 5.5 T for $H \parallel a$.

B. Reversible magnetization

Figure 2(a) shows raw magnetization curves measured down to 0.09 K in increasing and decreasing magnetic field applied parallel to the a axis. In the normal state, *i.e.* for $T = 4$ K, we find a large paramagnetic contribution with a field-independent susceptibility χ_a of about 4×10^{-4} in agreement with our previous study.¹⁷ At all temperatures, the magnetization is fully reversible over a wide field interval below the upper critical field $H_{c2}(T)$. This shows that our samples have very weak flux pinning, which is compatible with the recent observation of a well-defined hexagonal vortex lattice,²⁶ but is in strong contrast to more disordered Co-doped systems.^{27,28} Thus, accurate reversible magnetization data can be obtained by averaging the field increasing and decreasing branches of the magnetization loop, as shown in Fig.2(b). These curves clearly exhibit several features characteristic of strongly Pauli-limited superconductors.²⁹⁻³¹ First, $M(H)$ is negative, *i.e.* diamagnetic, only in a narrow low field interval $0 < H/H_{c2} < 0.3$ and positive, *i.e.* paramagnetic, for higher fields. Second, for the lowest temperature measured ($T = 0.09$ K), $M(H)$ increases strongly upon approaching $H_{c2}(T)$, rather than exhibiting the linear behavior expected from Ginzburg-Landau theory in the absence of paramagnetic effects. This is more clearly seen in Fig.2(c), where the normal-state magnetization has been subtracted. Similar behavior was already reported in both high- κ dirty Ti-V alloys ($\kappa \approx 68$)³² and clean CeCoIn_5 ($\kappa \approx 100$)^{29,30} and represent direct evidence for the existence of strong paramagnetic effects in KFe_2As_2 which become more and more important with decreasing temperatures.

The behavior of Pauli-limited superconductors was investigated theoretically in detail by Ichioka and Machida.^{33,34} In the inset of Fig.2(b), we show their calculations (at $T/T_c = 0.1$) for different values of the Maki parameter,

$$\alpha_M = \sqrt{2} \frac{H_{orb}(0)}{H_p(0)}, \quad (1)$$

(where $H_{orb}(0)$ and $H_p(0)$ are the zero-temperature values of the orbital and Pauli fields, respectively) which is a measure of the paramagnetic pair-breaking strength.³⁵ These theoretical curves clearly show that (i) the magnetization becomes rapidly positive with increasing field in the superconducting state with increasing α_M and (ii) the transition to the normal state at H_{c2} becomes first-order for large values of α_M . Our 0.09 K curve ($T/T_c \approx 0.03$) lies somewhere between the calculated curves for $\alpha_M = 1.7$ and 3.4 suggesting a weakly first-order transition at $T = 0$ K. Thus, our measurements clearly show, for the first time, the existence of strong paramagnetic depairing effects in KFe_2As_2 for $H \parallel a$. As shown in the inset of Fig.2(c), there is almost no paramagnetic effect for $H \parallel c$ and $\alpha_M \approx 0$ in this direction.

C. Thermodynamic critical field

Hereafter, we show that the thermodynamic critical field $H_c(T)$ obtained from the heat capacity data matches that obtained by our reversible magnetization measurements quite well. $H_c(T)$, which measures the Cooper-pairs condensation energy, can be determined directly from zero-field heat-capacity data using

$$-\frac{\mu_0}{2}H_c^2(T) = \int_0^T (S_s(T') - S_n(T'))dT', \quad (2)$$

(where S_n and S_s are the normal- and superconducting-state entropies, respectively) or using reversible magnetization curves with

$$-\frac{\mu_0}{2}H_c^2(T) = \mu_0 \int_0^{H_c} (M_s(T) - M_n(T))dH, \quad (3)$$

where M_n and M_s are the normal- and superconducting-state magnetizations, respectively. The resulting values of $H_c(T)$ (see Fig.3) inferred from magnetization data agree quite well with those calculated from the heat capacity, demonstrating the overall consistency between our thermodynamic measurements. It also indicates that the heat capacity is not contaminated by any spurious disordered magnetic contributions, as reported in Refs 25,36. In Section IV, we use the derived $H_c(T)$ to discuss the (H,T) phase diagram of KFe_2As_2 .

D. Thermal expansion and magnetostriction

We also performed thermal-expansion and magnetostriction measurements in order to study the effects of pressure, in particular uniaxial pressure, on the superconducting- and normal-state properties of KFe_2As_2 . Clear anomalies in the relative length changes $\Delta L_i/L_0$ ($i=a,c$) are seen at $T_c(H=0\text{ T}) = 3.4\text{ K}$ as shown in Fig.4(a) and (b). The red curves indicate the normal-state behavior, where superconductivity has been suppressed by a field of $H = 6\text{ T}$ applied along the a -axis, and the dashed lines indicate the extrapolated behavior down to $T = 0\text{ K}$.

The structural distortions in the superconducting state provide a direct indication of how the system can lower its free energy, and from these data it is clear that superconductivity favors a longer (shorter) a -axis (c -axis). Fig.4(c) - (f) show the corresponding uniaxial thermal-expansion coefficients $\alpha_i = (1/L_i)dL_i/dT$ ($i = a, c$), divided by temperature at different applied magnetic fields along the a -axis ((c) and (d)) and the c -axis ((e) and (f)). The anomalies at T_c have a clear step-like shape, indicating second-order phase transitions and decrease in temperature with increasing magnetic field.

Above T_c , α_i/T is constant and field independent, as expected for a Fermi liquid. Using Maxwell relations this

value is related to the pressure dependence of γ_n :²²

$$\frac{\alpha_i}{T} = -\frac{1}{V} \frac{\partial(\frac{S}{T})}{\partial p_i} = -\frac{1}{V_m} \frac{d\gamma_n}{dp_i}, \quad (4)$$

where $i=a,c$. The normal-state values of α_i/T are $\alpha_a/T = 0.12 \times 10^{-6}\text{ K}^{-2}$ and $\alpha_c/T = 0.08 \times 10^{-6}\text{ K}^{-2}$ which yield the following uniaxial-pressure dependencies of the normal-state Sommerfeld coefficients $d\gamma_n/dp_a = -7.74\text{ mJ mol}^{-1}\text{ K}^{-2}\text{ GPa}^{-1}$ and $d\gamma_n/dp_c = -4.81\text{ mJ mol}^{-1}\text{ K}^{-2}\text{ GPa}^{-1}$.

In order to determine the uniaxial-pressure dependencies of T_c , we use the Ehrenfest relation:^{21,37}

$$\frac{dT_c}{dp_i} = \frac{\Delta\alpha_i V_m}{\Delta C_p/T_c}, \quad (5)$$

where $i=a,c$. Here $\Delta\alpha_i$ is the jump in the thermal expansion along the i direction, $V_m = 61.27\text{ cm}^3\text{ mol}^{-1}$ is the molar volume and ΔC_p is the specific heat jump. Using our values for the thermal-expansion ($\Delta\alpha_a = -1.68 \times 10^{-6}\text{ K}^{-1}$ and $\Delta\alpha_c = 1.85 \times 10^{-6}\text{ K}^{-1}$) and heat-capacity ($\Delta C_p/T_c = 54\text{ mJ mol}^{-1}\text{ K}^{-2}$) jumps from Fig.1, we find $dT_c/dp_a = -1.92\text{ K GPa}^{-1}$ and $dT_c/dp_c = 2.10\text{ K GPa}^{-1}$. Our results show that the pressure dependence of T_c in KFe_2As_2 is very anisotropic. Indeed it is negative along the a -axis and positive along the c -axis, although the magnitudes are comparable. Interestingly, superconductivity couples strongly to the c/a ratio as in Co- and P-doped Ba122,^{21,23} but with opposite sign, *i.e.* a smaller, rather than a larger, c/a ratio enhances T_c . Under hydrostatic conditions we get a negative $dT_c/dp_{vol} = 2dT_c/dp_a + dT_c/dp_c = -1.74\text{ K GPa}^{-1}$. Our results are in qualitative agreement with the recent data of Bud'ko *et al.*,³⁸ who find $dT_c/dp_{vol} = -1.0\text{ K GPa}^{-1}$, $dT_c/dp_a \approx -1.1\text{ K GPa}^{-1}$ and $dT_c/dp_c \approx 1.1\text{ K GPa}^{-1}$ from hydrostatic pressure and c -axis thermal expansion data.

The pressure dependence of the thermodynamic critical field can be calculated using the following relation:³⁹

$$\frac{\Delta L_i}{L_i} = \frac{L_{n,i} - L_{s,i}}{L_{s,i}} = \mu_0 H_c \left(\frac{dH_c}{dp_i} \right), \quad (6)$$

where $i = a, c$ and $\Delta L_i/L_i$ are the relative length changes from Fig.4. We obtain $dH_c^a/dp_a = -0.049\text{ T GPa}^{-1}$ and $dH_c^a/dp_c = 0.046\text{ T GPa}^{-1}$.

Additional information about how uniaxial pressure affects both the normal- and superconducting-state properties of KFe_2As_2 can be obtained from magnetostriction measurements. The magnetostriction coefficients λ_i are directly related to the uniaxial pressure dependences of the magnetization via

$$\lambda_i = \frac{1}{L_i} \frac{dL_i}{dH} = -\frac{dM}{dp_i}, \quad (7)$$

where $i = a, c$. Figure 5 shows the magnetostriction data for various samples and field orientations for temperatures between 1.7 K and 4 K. The pressure dependence

of the normal-state Pauli susceptibility can be directly obtained from $\lambda(H)$ for $H > H_{c2}$, which also varies linearly with field strength (see Fig.5(c), (d), (g), (h)) from Eq.7. With this we extract $d\chi^a/dp_a = -1.43 \times 10^{-5} \text{ GPa}^{-1}$, $d\chi^c/dp_a = 4.13 \times 10^{-6} \text{ GPa}^{-1}$, $d\chi^a/dp_c = -6.74 \times 10^{-6} \text{ GPa}^{-1}$, and $d\chi^c/dp_c = -3.08 \times 10^{-5} \text{ GPa}^{-1}$. Interestingly, the biggest effects of uniaxial pressure on the magnetic susceptibility occur when the applied magnetic field is parallel to the pressure direction and is nearly one order of magnitude weaker for different orientations.

The magnetostriction below T_c is fully reversible and thus, also provides information about how the reversible magnetization responds to uniaxial pressure.^{40,41} The reversible magnetostriction depends basically on two parameters, H_c and the Ginzburg-Landau parameter κ , both of which can be pressure dependent. From the shape of $\lambda(H)$, it is evident that the main contribution to the magnetostriction comes from dH_c/dp_i and not from $d\kappa/dp_i$ for both field directions.⁴¹ For example, if $d\kappa/dp_i$ were the primary pressure derivative, $\lambda_i(H)$ would change sign near $H_{c2}/2$,⁴¹ which is clearly not the behavior found in our data. For Pauli-limited superconductors, the Maki parameter may also be pressure dependent, complicating this simple analysis at high fields. Indeed, for $H \parallel a$, we observe a strong increase in the size of the magnetostriction anomaly with decreasing temperatures, which is not expected for conventional superconductors.^{40,41} Since $\lambda(H)$ is directly proportional to the pressure derivative of $M(H)$ (see Eq.7), this increase in the $\lambda(H)$ anomaly directly reflects of the changing shape of the $M(H)$ curve at low temperatures and signals the crossover to a strongly Pauli-limited superconductor as the temperature is lowered.⁴² We also find an anomalous increase in the size of the expansivity anomaly for fields above about 3 T (see Fig.4(d)) which is also directly related to the onset of strong paramagnetic depairing for $H \parallel a$.

IV. DISCUSSION

A. (H,T) phase diagram and paramagnetic effects

Figure 6 shows the superconducting (H,T) phase diagram of KFe_2As_2 derived from our thermodynamic measurements, which is similar to other results.^{6,42,43} As expected, $H_{c2}(T)$ is linear in the vicinity of T_c for both field orientations, since the suppression of superconductivity in this region is always governed by the orbital effect. However, with decreasing temperature, it clearly flattens for $H \parallel a$, which corroborates the importance of paramagnetic depairing in this layered compound, already inferred from our magnetization curves. We note that a similar behavior is observed for nearly optimally K doped samples.⁴⁴ Although our heat-capacity data exhibit clear signs of multiband superconductivity (see Fig.1), we find no evidence of a sizeable change of curvature at high temperature due to the existence of several

energy gaps, as reported in MgB_2 for $H \perp c$.⁴⁵ The initial slopes $(\partial H_{c2}/\partial T)_{T_c}$ are equal to -0.6 and -3.7 T K⁻¹ for $H \parallel c$ and $H \parallel a$, respectively in agreement with the values of Terashima *et al.*⁶ which lead to the coherence lengths $\xi_{GL}^{ab} \approx 13 \text{ nm}$ and $\xi_{GL}^c \approx 2 \text{ nm}$. Using these values, we calculate the temperature dependence of the orbital field $H_{orb}(T)$ for both directions using the Helfand-Werthamer theory⁴⁶⁻⁴⁸ in the clean limit. As shown in Fig.6, $H_{c2}(T)$ is fully orbitally limited with $H_{c2}(0) = H_{orb}^c(0) \approx 1.5 \text{ T}$. For $H \parallel a$, Zeeman effects start to become significant below about 2.8 K and at $T = 0 \text{ K}$, we find $H_{orb}^{ab}(0) \approx 9 \text{ T}$ *i.e.* significantly larger than the measured $H_{c2}(0) \approx 5 \text{ T}$. Using $H_c(0) = 73 \text{ mT}$ (see Fig.3), we estimate the Maki-Ginzburg-Landau parameter $\kappa_1 = \frac{H_{orb}(0)}{\sqrt{2} \cdot H_c(0)}$ equal to 87 and 15 for $H \parallel a$ and $H \parallel c$, respectively. This shows that KFe_2As_2 is a very strong type II superconductor especially for $H \parallel a$. This is expected since paramagnetic effects are significant only in strong type II superconductors, in which the magnetic field strongly penetrates the sample. The Pauli field $H_p(0)$, *i.e.* the field at which the difference of Zeeman energy between the normal- and superconducting states exactly compensates the Cooper-pairs condensation energy, can be written in the following way⁴⁹

$$H_p(0) = \frac{H_c(0)}{\sqrt{\chi_n - \chi_s}}, \quad (8)$$

Here χ_n and χ_s are the spin susceptibilities in the normal- and superconducting states, respectively. In the single-band *s*-wave case, $\chi_s = 0$ and $H_p(0) = 3.6 \text{ T}$ (3.9 T) are obtained for $H \parallel a$ ($H \parallel c$). Here, we have used the values of χ_n obtained in Ref. 17 (assuming implicitly that χ_n is dominated by the Pauli paramagnetism) and our value of $H_c(0)$. The above estimation, which is smaller than the measured $H_{c2}(0)$ for $H \parallel a$, only provides a lower limit of the Pauli field, and $H_p(0)$ can be enhanced by *e.g.* strong-coupling effects,⁵⁰ nodal gaps,⁵¹ or multiband superconductivity⁵². In KFe_2As_2 , an enhancement of $H_p(0)$ by strong coupling can be discarded since $\Delta C_p/\gamma_n T_c \approx 0.54$ is substantially smaller than the single-band BCS value 1.43, in contrast to $\text{Ba}_{0.68}\text{K}_{0.32}\text{Fe}_2\text{As}_2$ where $\Delta C_p/C_p \approx 2.5$.⁸ The response of a nodal superconductor to a magnetic field is quite different to that of a *s*-wave because the unpaired electrons located in the regions where the Zeeman field exceeds the local gap $\Delta(\mathbf{k})$ can be spin-polarized.⁵¹ Thus, χ_s is not zero and superconductivity can sustain a higher paramagnetic field. However, in this case $\chi_s \approx 0.19 \cdot \chi_n$,⁵³ (neglecting the small field dependence of the gap) and $H_p(0)$ is only slightly enhanced to 4 T for $H \parallel a$, which is still less than the observed $H_{c2}(0)$. A significantly larger enhancement can be obtained in multiband superconductors with widely different gap amplitudes, *i.e.* $\Delta_2 \gg \Delta_1$.^{52,54} In this scenario, the band with the smaller gap will almost recover its normal-state density of states, $N_1(0)$, for $H > \Delta_1(0)$, while the second band, with the larger gap, will remain gapped all the way up to $H_p(0)$ where $\chi_s = \frac{N_1(0)}{N_1(0) + N_2(0)} \cdot \chi_n$. For in-

TABLE I: Normal- and superconducting-state parameters of KFe_2As_2

	H a	H c
γ_n (mJ mol ⁻¹ K ⁻²)	103	
T_c (K)	3.4	
χ_n	4.1×10^{-4}	3.2×10^{-4}
κ_1	87	15
$H_c(0)$ (T)	0.073	
$(\partial H_{c2}/\partial T)_{T_c}$ (T K ⁻¹)	-3.7	-0.6
$H_{c2}(0)$ (T)	5	1.5
$H_{orb}(0)$ (T)	9	1.5
$H_p(0)$ (T)	6.7	
α_M	1.8	0.3

stance, $H_p(0)$ would be enhanced by a factor of about 1.4 for $N_1 = N_2$. However, an accurate value of $H_p(0)$ from Eq. 8 cannot be derived at present because the Fermi-surface of KFe_2As_2 consists of 4 sheets and all the gaps and densities of states have not been determined yet. Since the large gap ultimately determined $H_{c2}(0)$, an approximate value can nevertheless be obtained using the following expression

$$\frac{H_{c2}(\alpha_M)}{H_{orb}(0)} = \frac{1}{\sqrt{1 + 0.6 \cdot \alpha_M^2}}, \quad (9)$$

derived by Machida and Ichioka^{34,55} for a single band superconductor in the clean limit. For H || *a*, we find $H_{c2}(0)/H_{orb}(0) \approx 0.6$ which gives $\alpha_M \approx 1.8$, in good agreement with our simple estimate (see Section III B and inset of Fig.2(b)). We note that this corresponds roughly to the minimum value that allows the formation of the FFLO phase in the presence of orbital effects,⁵⁶ and warrants more low temperature measurements on this system. Our estimated values for all these fields are summarized in Table I.

B. Uniaxial pressure effects

A summary of the uniaxial pressure derivatives is given in Table II; here we have also included the relative pressure derivatives, which allows us to directly compare the magnitude of the various derivatives. The largest relative pressure derivatives are for T_c and H_c , which are roughly equal both in magnitude and sign. Thus, the critical temperature and the condensation energy are strongly linked, which is not surprising. On the other hand, the relative pressure derivative of γ_n and χ are much smaller than those of T_c and H_c . Also, there is no direct correlation

between the signs of dT_c/dp_i and $d\gamma_n/dp_i$, which implies that these quantities are not directly related. Here it is worth pointing out that pressure and doping are strongly correlated in Co- and P-doped systems,^{22,23} which manifests itself in a similar dependence of T_c and γ_n versus either doping or pressure. Such a correlation between doping and pressure does not appear to work for the K-doped systems. Indeed, γ_n is largest and T_c is lowest for KFe_2As_2 . Thus, if a similar equivalence would hold, one would expect that under hydrostatic pressure γ_n would increase since T_c decreases, which is the opposite of the observed behavior (see Table II). Using a bulk elastic modulus from the DFT calculation of $B = 45$ GPa,⁵⁷ we can also calculate volume Grüneisen parameters of the various physical quantities (see Table II). Interestingly, these volume Grüneisen parameters of T_c and γ_n are of similar magnitude and sign as found in various U-based heavy fermion materials,⁵⁸ which was interpreted in terms of a negative pressure dependence of the pairing interaction. Similar physics may be operating in KFe_2As_2 , which may be considered 3*d* heavy fermion metal.¹⁷

V. CONCLUSIONS

In conclusion, the present thermodynamic investigation of KFe_2As_2 has revealed several interesting results. Clear evidence for strong Pauli-limiting behavior is observed in the low-temperature magnetization measurements. Further detailed studies are needed to determine if the low-temperature transition is effectively first-order and for searching for other ordering phenomena, such as the elusive FFLO state. Interestingly, the derived uniaxial pressure derivatives show that superconductivity in KFe_2As_2 responds strongly to the *c/a* ratio of the lattice constants, but with the opposite sign as in Co- and P-doped Ba122 iron pnictides, showing that this is not a universal characteristic of these materials. It is hoped that the various pressure derivatives derived here will add a stringent constraint on superconducting theories of this interesting low- T_c compound.

Acknowledgments

The authors thank J. Schmalian, I. Vekhter, K. Machida and M. Ichioka for useful discussions. This work has been supported by the DFG through SPP1458. The work performed in Grenoble was supported by the French ANR Projects SINUS and CHIRnMAG and the ERC starting grant NewHeavyFermion.

¹ D. C. Johnston, Adv. Phys. **59**, 803 (2010).

² J. Paglione and R. L. Greene, Nat. Phys. **6**, 645 (2010).

TABLE II: Table of uniaxial pressure dependencies along the a - and the c -axis, the corresponding normalized pressure dependencies in units of GPa^{-1} and the Grüneisen parameters. Values of χ^a and χ^c are taken from Ref.¹⁷.

	$\gamma_n = 102 \text{ mJ mol}^{-1}\text{K}^{-2}$	$T_c = 3.45 \text{ K}$	$\chi^a = 4.1 \times 10^{-4}$	$\chi^c = 3.2 \times 10^{-4}$	$H_c^a = 0.72 \text{ T}$
	$d\gamma_n/dp_i [\text{mJ mol}^{-1}\text{K}^{-2}\text{GPa}^{-1}]$	$dT_c/dp_i [\text{K GPa}^{-1}]$	$d\chi^a/dp_i [\text{GPa}^{-1}]$	$d\chi^c/dp_i [\text{GPa}^{-1}]$	$dH_c^a/dp_i [\text{T GPa}^{-1}]$
a -axis	-7.74	-1.92	-1.43×10^{-5}	4.13×10^{-6}	-0.049
c -axis	-4.81	2.10	-6.74×10^{-6}	-3.08×10^{-5}	0.046
	$d \ln \gamma_n / dp_i$	$d \ln T_c / dp_i$	$d \ln \chi^a / dp_i$	$d \ln \chi^c / dp_i$	$d \ln H_c^a / dp_i$
a -axis	-0.076	-0.56	-0.035	0.013	-0.709
c -axis	-0.047	0.61	-0.016	-0.096	0.664
Volume	-0.199	-0.51	-0.086	-0.070	-0.754
Grüneisen parameter	$d \ln \gamma_n / d \ln V$	$d \ln T_c / d \ln V$	$d \ln \chi^a / d \ln V$	$d \ln \chi^c / d \ln V$	$d \ln H_c^a / d \ln V$
Volume	-8.9	-22.9	-3.9	-3.1	-33.9

- ³ G. R. Stewart, Rev. Mod. Phys. **83**, 1589 (2011).
- ⁴ I. I. Mazin and J. Schmalian, Physica C **469**, 614 (2009).
- ⁵ H. Fukazawa, Y. Yamada, K. Kondo, T. Saito, Y. Kohori, K. Kuga, Y. Matsumoto, S. Nakatsuji, H. Kito, P. M. Shirage, et al., J. Phys. Soc. Jpn **78**, 083712 (2009).
- ⁶ T. Terashima, M. Kimata, H. Satsukawa, A. Harada, K. Hazama, S. Uji, H. Harima, G.-F. Chen, J.-L. Luo, and N.-L. Wang, J. Phys. Soc. Jpn **78**, 063702 (2009).
- ⁷ M. Rotter, M. Tegel, and D. Johrendt, Phys. Rev. Lett. **101**, 107006 (2008).
- ⁸ P. Popovich, A. V. Boris, O. V. Dolgov, A. A. Golubov, D. L. Sun, C. T. Lin, R. K. Kremer, and B. Keimer, Phys. Rev. Lett. **105**, 027003 (2010).
- ⁹ Z. Li, D. L. Sun, C. T. Lin, Y. H. Su, J. P. Hu, and G. Q. Zheng, Phys. Rev. B **83**, 140506 (2011).
- ¹⁰ R. Thomale, C. Platt, W. Hanke, J. Hu, and B. A. Bernevig, Phys. Rev. Lett. **107**, 117001 (2011).
- ¹¹ K. Hashimoto, A. Serafin, S. Tonegawa, R. Katsumata, R. Okazaki, T. Saito, H. Fukazawa, Y. Kohori, K. Kihou, C. H. Lee, et al., Phys. Rev. B **82**, 014526 (2010).
- ¹² J.-P. Reid, M. A. Tanatar, A. Juneau-Fecteau, R. T. Gordon, S. R. de Cotret, N. Doiron-Leyraud, T. Saito, H. Fukazawa, Y. Kohori, K. Kihou, et al., Phys. Rev. Lett. **109**, 087001 (2012).
- ¹³ K. Okazaki, Y. Ota, Y. Kotani, W. Malaeb, Y. Ishida, T. Shimojima, T. Kiss, S. Watanabe, C.-T. Chen, K. Kihou, et al., Science **337**, 1314 (2012).
- ¹⁴ T. Sato, K. Nakayama, Y. Sekiba, P. Richard, Y.-M. Xu, S. Souma, T. Takahashi, G. F. Chen, J. L. Luo, N. L. Wang, et al., Phys. Rev. Lett. **103**, 047002 (2009).
- ¹⁵ C. H. Lee, K. Kihou, H. Kawano-Furukawa, T. Saito, A. Iyo, H. Eisaki, H. Fukazawa, Y. Kohori, K. Suzuki, H. Usui, et al., Phys. Rev. Lett. **106**, 067003 (2011).
- ¹⁶ J.-P. Castellan, S. Rosenkranz, E. A. Goremychkin, D. Y. Chung, I. S. Todorov, M. G. Kanatzidis, I. Eremin, J. Knolle, A. V. Chubukov, S. Maiti, et al., Phys. Rev. Lett. **107**, 177003 (2011).
- ¹⁷ F. Hardy, A. Böhmer, D. Aoki, P. Burger, T. Wolf, P. Schweiss, R. Heid, P. Adelmann, Y. Yao, G. Kotliar, et al., ArXiv e-prints **1302.1696** (2013).
- ¹⁸ L. de' Medici, G. Giovannetti, and M. Capone, ArXiv e-prints **1212.3966** (2012).
- ¹⁹ P. P. Fulde and R. A. Ferrell, Phys. Rev. **135**, A550 (1964).
- ²⁰ A. I. Larkin and Y. N. Ovchinnikov, Sov. Phys. JETP **20**, 762 (1965).
- ²¹ F. Hardy, P. Adelmann, T. Wolf, H. v. Löhneysen, and C. Meingast, Phys. Rev. Lett. **102**, 187004 (2009).
- ²² C. Meingast, F. Hardy, R. Heid, P. Adelmann, A. Böhmer, P. Burger, D. Ernst, R. Fromknecht, P. Schweiss, and T. Wolf, Phys. Rev. Lett. **108**, 177004 (2012).
- ²³ A. E. Böhmer, P. Burger, F. Hardy, T. Wolf, P. Schweiss, R. Fromknecht, H. v. Löhneysen, C. Meingast, H. K. Mak, R. Lortz, et al., Phys. Rev. B **86**, 094521 (2012).
- ²⁴ C. Meingast, B. Blank, H. Bürkle, B. Obst, T. Wolf, H. Wühl, V. Selvamanickam, and K. Salama, Phys. Rev. B **41**, 11299 (1990).
- ²⁵ V. Grinenko, S.-L. Drechsler, M. Abdel-Hafiez, S. Aswartham, A. U. B. Wolter, S. Wurmehl, C. Hess, K. Nenkov, G. Fuchs, D. V. Efremov, et al., Phys. Status Solidi B **250**, 593 (2013).
- ²⁶ H. Kawano-Furukawa, C. J. Powell, J. S. White, R. W. Heslop, A. S. Cameron, E. M. Forgan, K. Kihou, C. H. Lee, A. Iyo, H. Eisaki, et al., Phys. Rev. B **84**, 024507 (2011).
- ²⁷ M. R. Eskildsen, L. Y. Vinnikov, T. D. Blasius, I. S. Veshchunov, T. M. Artemova, J. M. Densmore, C. D. Dewhurst, N. Ni, A. Kreyssig, S. L. Bud'ko, et al., Phys. Rev. B **79**, 100501 (2009).
- ²⁸ A. Yamamoto, J. Jaroszynski, C. Tarantini, L. Balicas, J. Jiang, A. Gurevich, D. C. Larbalestier, R. Jin, A. S. Sefat, M. A. McGuire, et al., Appl. Phys. Lett. **94**, 062511 (2009).
- ²⁹ T. Tayama, A. Harita, T. Sakakibara, Y. Haga, H. Shishido, R. Settai, and Y. Onuki, J. Phys. Chem. Solids **63**, 1155 (2002).
- ³⁰ C. Paulsen, D. Aoki, G. Knebel, and J. Flouquet, J. Phys. Soc. Jpn. **80**, 053701 (2011).
- ³¹ K. Tenya, S. Yasuda, M. Yokoyama, H. Amitsuka, K. Deguchi, and Y. Maeno, Physica B **378**, 495 (2006).
- ³² R. R. Hake, Phys. Rev. **158**, 356 (1967).
- ³³ M. Ichioka, K. M. Suzuki, Y. Tsutsumi, and K. Machida, *Superconductivity - Theory and Applications* (In-Tech, 2011), chap. 10.
- ³⁴ M. Ichioka and K. Machida, Phys. Rev. B **76**, 064502 (2007).
- ³⁵ K. Maki, Physics **1**, 127 (1964).

- ³⁶ M. Abdel-Hafiez, S. Aswartham, S. Wurmehl, V. Grinenko, C. Hess, S. L. Drechsler, S. Johnston, A. U. B. Wolter, B. Büchner, H. Rosner, et al., *Phys. Rev. B* **85**, 134533 (2012).
- ³⁷ P. Ehrenfest, *Mitteilungen aus dem Kammerlingh Onnes-Institut Leiden* **75b**, 628 (1938).
- ³⁸ S. L. Bud'ko, Y. Liu, T. A. Lograsso, and P. C. Canfield, *Phys. Rev. B* **86**, 224514 (2012).
- ³⁹ D. Shoenberg, *Superconductivity* (Cambridge University Press, 1962).
- ⁴⁰ G. Brändli and F. D. Enck, *Phys. Lett. A* **26**, 360 (1968).
- ⁴¹ P. Popovych, Ph.D. thesis, Universität Karlsruhe (TH) (2006).
- ⁴² D. A. Zocco, K. Grube, F. Eilers, T. Wolf, and H. v. Löhneysen, *ArXiv e-prints* **1305.5130** (2013).
- ⁴³ Y. Liu, M. A. Tanatar, V. G. Kogan, H. Kim, T. A. Lograsso, and R. Prozorov, *Phys. Rev. B* **87**, 134513 (2013).
- ⁴⁴ M. M. Altarawneh, K. Collar, C. H. Mielke, N. Ni, S. L. Bud'ko, and P. C. Canfield, *Phys. Rev. B* **78**, 220505 (2008).
- ⁴⁵ L. Lyard, P. Szabó, T. Klein, J. Marcus, C. Marcenat, K. H. Kim, B. W. Kang, H. S. Lee, and S. I. Lee, *Phys. Rev. Lett.* **92**, 057001 (2004).
- ⁴⁶ E. Helfand and N. R. Werthamer, *Phys. Rev. Lett.* **13**, 686 (1964).
- ⁴⁷ E. Helfand and N. R. Werthamer, *Phys. Rev.* **147**, 288 (1966).
- ⁴⁸ J. P. Brison, N. Keller, A. Verniere, P. Lejay, L. Schmidt, A. Buzdin, J. Flouquet, S. R. Julian, and G. G. Lonzarich, *Physica C* **250**, 128 (1995).
- ⁴⁹ D. Saint-James, E. J. Thomas, and G. Sarma, *Type II Superconductivity* (Pergamon Press, 1969).
- ⁵⁰ T. P. Orlando, J. E. J. McNiff, S. Foner, and M. R. Beasley, *Phys. Rev. B* **19**, 4545 (1979).
- ⁵¹ K. Yang and S. L. Sondhi, *Phys. Rev. B* **57**, 8566 (1998).
- ⁵² V. Barzykin, *Phys. Rev. B* **79**, 134517 (2009).
- ⁵³ H. Won, H. Jang, and K. Maki, *ArXiv e-prints* **9901252** (1999).
- ⁵⁴ V. Barzykin and L. P. Gor'kov, *Phys. Rev. Lett.* **98**, 087004 (2007).
- ⁵⁵ K. Machida and M. Ichioka, *Phys. Rev. B* **77**, 184515 (2008).
- ⁵⁶ L. W. Gruenberg and L. Gunther, *Phys. Rev. Lett.* **16**, 996 (1966).
- ⁵⁷ R. Heid, unpublished (2013).
- ⁵⁸ J. Flouquet, J. Brison, K. Hasselbach, L. Taillefer, K. Behnia, D. Jaccard, and A. de Visser, *Physica C* **185**, 372 (1991).

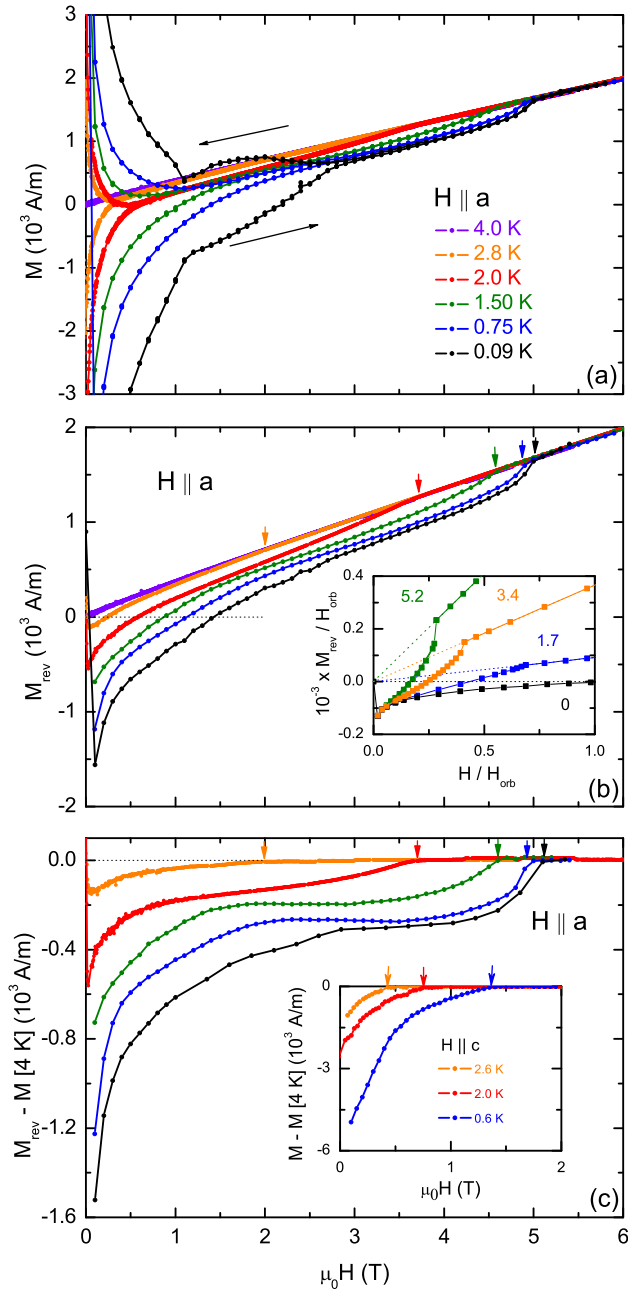


FIG. 2: (Color Online) (a) Magnetization curves for $H \parallel a$ at different temperatures. (b) Reversible part of the magnetization. The inset shows calculations from Ichioka and Machida^{33,34} for several values of α_M (for $\alpha_M > 1.8$, transitions are 1st order). (c) Difference between the reversible superconducting- and normal-state magnetizations. The inset shows data for $H \parallel c$ at several temperatures. The arrows indicate the values of H_{c2} (T).

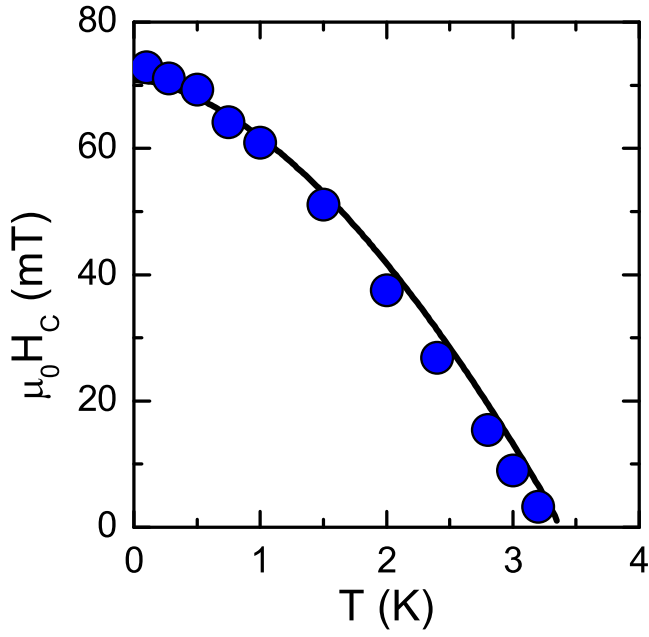


FIG. 3: (Color Online) Temperature dependence of the thermodynamic critical field inferred from specific-heat (line) and magnetization (symbol) measurements.

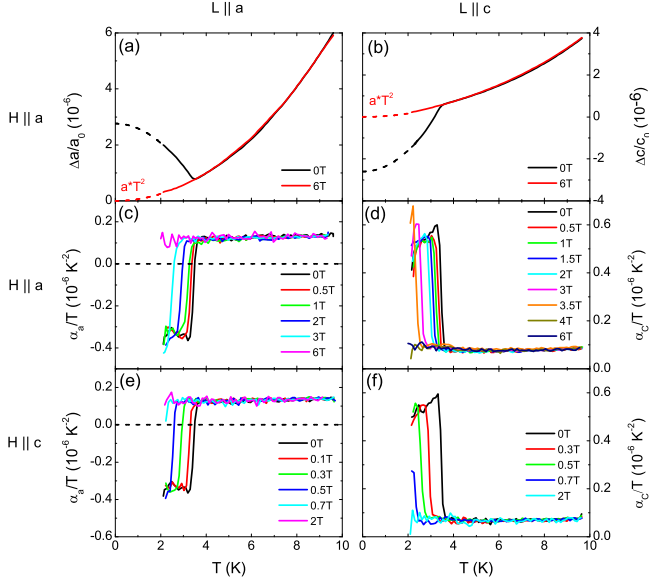


FIG. 4: (Color Online) (a) Relative length change versus temperature of the a -axis (b) and c -axis in the normal (red curves) and the superconducting state (black curves). (c) - (f) Uniaxial thermal-expansion coefficients divided by temperature $\alpha_{a,c}/T$ as a function of temperature for both crystallographic axes and different fields.

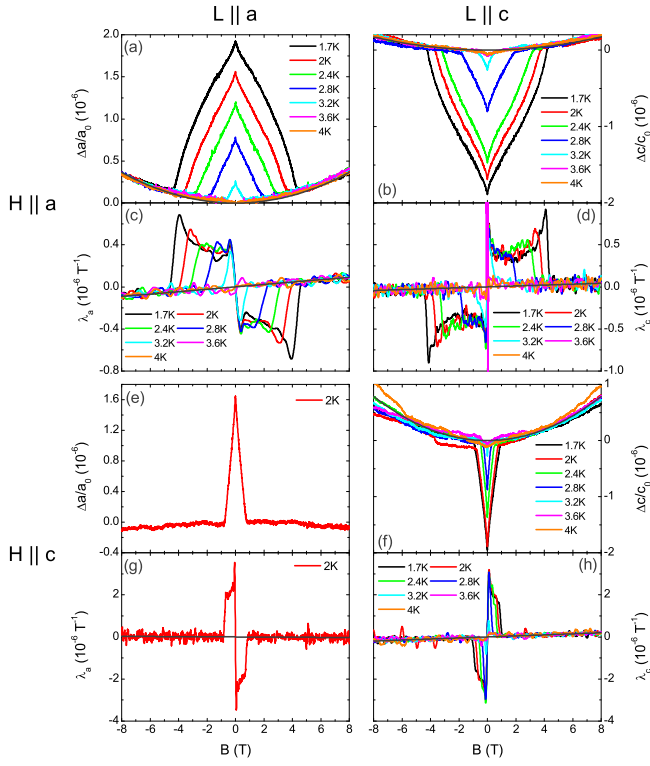


FIG. 5: (Color Online) Magnetostriction $\Delta L_i(H)/L_0$ ($i = a, c$) and linear magnetostriction coefficients $\lambda_i(H)$ for the a - (left side) and c -axis (right side) for different field orientations. For $H \parallel a$, the anomaly in $\lambda_i(H)$ at H_{c2} increases strongly in magnitude with decreasing temperature (see (c) and (d)) due to the onset of Pauli-limiting behavior, whereas for $H \parallel c$ (see (g) and (h)), such an increase is notably absent.

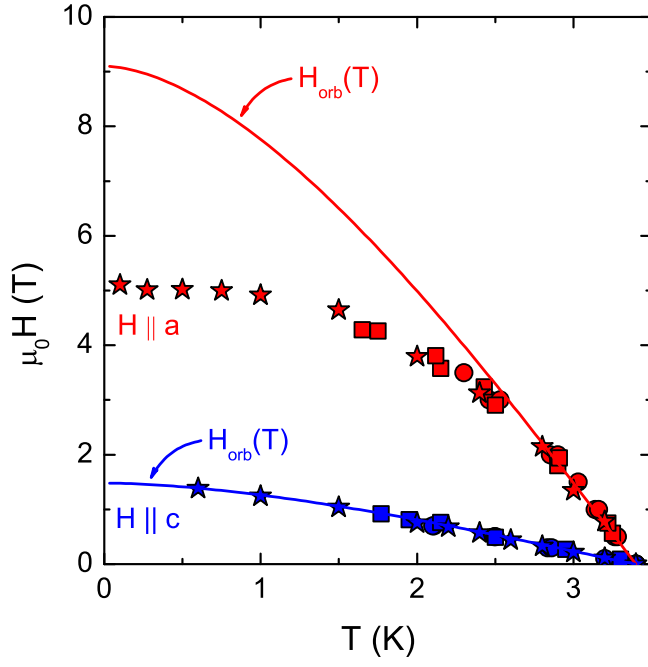


FIG. 6: (Color Online) (H,T) phase diagram of KFe_2As_2 derived from magnetization (\star), thermal-expansion (\circ) and magnetostriction measurements (\square). Solid lines are the orbital fields calculated using the clean-limit Helfand-Werthamer theory. A strong suppression of H_{c2} due to Pauli depairing is observed for $H \parallel a$.